Journal of Applied Polymer Science

WILEY

Journal of Applied Polymer Science

RESEARCH ARTICLE

Copula-Based Data Augmentation and Machine Learning for Predicting Tensile Strength of 3D-Printed PLA Under Anisotropic Conditions

Ahmet Saylık[1] | Ertan Kösedağ[2] | Taha Etem[3]

[1]Department of Mechanical Engineering, Mus Alparslan University, Mus, Turkey | [2]Department of Mechanical Engineering, Van Yuzuncu Yil University, Van, Turkey | [3]Department of Computer Engineering, Cankiri Karatekin University, Cankiri, Turkey

Correspondence: Ahmet Saylık (a.saylik@alparslan.edu.tr)

Received: 2 May 2025 | **Revised:** 4 June 2025 | **Accepted:** 19 June 2025

Funding: The authors received no specific funding for this work.

Keywords: applications | manufacturing | mechanical properties | thermoplastics

ABSTRACT

In this study, 48 polylactic acid (PLA) samples were produced via 3D printing, incorporating four infill geometries (gyroid, lattice, honeycomb, and linear), four infill rates (15%–60%), and three printing directions (x, y, z). Tensile testing revealed anisotropic mechanical behavior, with the x-direction consistently outperforming y- and z-directions due to layer adhesion dynamics. A machine learning framework leveraging copula-based data augmentation was developed to predict tensile strength at untested infill rates. The framework employed least squares regression, support vector machines (SVM), Gaussian process regression (GPR), and artificial neural networks (ANNs), augmented with 20,000 synthetic data points to enhance model robustness. Results demonstrated that gyroid geometry in the x-direction achieved the highest tensile strength (53.4 MPa at 60% infill), while Lattice patterns underperformed. Data augmentation improved prediction accuracy across all models, with SVM achieving the lowest RMSE (1.53 MPa) and R^2 values exceeding 0.87. This study highlights the critical interplay of infill parameters, directional anisotropy, and machine learning in optimizing 3D-printed PLA components for industrial applications, offering a data-driven pathway to reduce experimental costs and accelerate material design.

1 | Introduction

Polymer-based 3D printers, particularly due to their advantages such as lightness, design flexibility, and low production costs, are preferred in the industry. Today, 3D-printing technologies are used across a wide range of fields, from engineering applications, healthcare and biomedicine, aerospace, automotive, architecture and construction, education and research, defense and security, to food technology [1–6]. The extrusion of material produced by a 3D printer is a layer-based additive manufacturing (AM) technique also known as fused deposition modeling (FDM) or fused filament fabrication (FFF) [7]. This manufacturing process begins with model preparation using CAD (computer-aided design) software to create a 3D model, which is then transferred to a 3D printer to produce materials in the desired geometry [8–12]. The printed materials from 3D printing demonstrate all-encompassing changes in their mechanical properties based on multiple factors involving print parameter settings and material content with geometric features [13, 14]. The variations between material specifications create uncertainties that affect the manufacturing methods and engineering reliability functions. Studies have merged research on 3D and 4D printer processes and materials and printing methods with machine learning explorations to establish how machine learning would help quality management, along with fault identification and process optimization [15]. Studies have

[Correction added on August 19, 2025, after first online publication: The copyright line was changed.]

proven that machine learning prediction methods produce results at a 70% faster rate compared to conventional experimental methods [16]. Predicting the mechanical properties of various geometric structures in 3D printing through machine learning approaches constitutes a vital field of current material science research for manufacturing optimization. Five different machine learning algorithms that examined linear regression, random forest regression, AdaBoost regression, gradient boosting regression, and XGBoost regression provided comparison between their effectiveness for 3D-printing material tensile strength prediction [17]. Research was conducted on the accuracy assessment on four supervised machine learning models for ultimate tensile strength (UTS) prediction of FDM-printed PLA samples, which revealed K-nearest neighbors (KNN) to be the most accurate predictor [18]. Mishra et al. (2024) employed KNN to estimate UTS of PLA, achieving 94% accuracy but overlooking directional anisotropy. Diverse ensemble learning tools produced predictions for the tensile strength and Young's modulus, and elongation at break of PLA and PLA-CF FFF-produced samples, which demonstrated accuracies of 91.75%, 94.08%, and 88.54% respectively [19]. A study of printing parameters layered with thickness and infill amount alongside printing speed and temperature evaluated FDM-produced PLA parts and used machine learning models for predicting mechanical properties to find the optimal print settings [20, 21]. Controllers predicted the mechanical properties of FDM-produced PLA materials through their analysis of fuzzy logic and artificial neural network (ANN) models, which displayed varying prediction precision levels. An ANN became the most effective model when tested against other models, where its accuracy reached 94% [22]. The XGBoost model delivered the best results when predicting tensile strength values of PLA samples manufactured through FDM because it accomplished a 96% accuracy level in this prediction task [23]. Experiments of the Taguchi method resulted in a set of experiments for predicting PLA material tensile strength, which delivered valid results with measurement precision lower than 5% [24]. Recent advances in FDM have spurred extensive research into optimizing the mechanical properties of 3D-printed polylactic acid (PLA). Karimi et al. (2024) explored continuous-fiber-reinforced composites, revealing that infill patterns like gyroid enhance stress distribution, though computational modeling gaps persist [25]. Wawryniuk et al. (2024) highlighted anisotropic behavior in aerospace-grade PLA, with x-direction printing yielding 15%–25% higher strength than z-direction counterparts, attributed to interlayer bonding dynamics [26]. Ozdemir et al. evaluated the print quality by performing 3D printing at different temperatures and flow rates. In order to optimize this printing process, a model that predicts printability and print quality using machine learning (random forest algorithm) was able to successfully predict the print quality with 92.8% accuracy by analyzing the complex relationships between material properties and printing parameters [27].

Recent advancements at the intersection of machine learning and AM have led to significant improvements in process optimization, quality control, and material characterization. For instance, a study by Hamrani et al. systematically reviews the application of machine learning in wire arc AM, highlighting its potential in enhancing process efficiency and product quality [28]. Similarly, Zhang et al. developed a machine learning framework to predict melt pool morphology in laser-based powder bed fusion processes, achieving high accuracy in forecasting melt pool area and shape, which is crucial for ensuring consistent build quality [29]. In another comprehensive review, Saimon et al. explored the integration of deep learning in AM, discussing current progress and future challenges, particularly in design, modeling, and real-time monitoring [30]. Furthermore, Karimzadeh et al. reviewed machine learning methods for fabricating functionally graded materials via AM, addressing challenges such as parameter optimization and defect detection [31]. Lastly, Peles et al. introduced a deep-learning approach for quantitative structural characterization in AM, enabling rapid and accurate predictions of geometric features like melt pool boundaries and defects [32]. Kazmi et al. implemented ML algorithms, including ANN and XGBoost, in robotic wire arc AM to minimize surface roughness, finding that these models effectively predict and improve the quality of deposited aluminum alloy beads [33]. Kumar et al. provided a comprehensive review of ML applications across various stages of AM, such as design, process optimization, and production control, highlighting the potential of ML to revolutionize manufacturing efficiency and product quality [34]. Sing et al. discussed the integration of ML in laser powder bed fusion for metal AM, emphasizing its role in enhancing process monitoring, defect detection, and overall part quality [35]. Jiang conducted a survey on ML applications in AM technologies, offering insights into current trends and future directions, particularly in process parameter optimization and real-time monitoring [36]. Additionally, a comprehensive review explored the integration of ML into AM of metallic biomaterials, focusing on advancements in design, process optimization, and quality control, underscoring the transformative potential of ML in biomedical applications [37]. Several studies have highlighted that the mechanical and thermal performance of recycled polymer filaments can be effectively optimized through tailored processing strategies. Recycled PLA (Re-PLA), for instance, has been shown to retain acceptable tensile strength levels under optimized FDM parameters, such as increased infill density and layer thickness [38]. Furthermore, significant improvements in mechanical strength have been reported for filaments reinforced with high-performance additives such as carbon or glass fibers [39]. Nevertheless, recycled thermoplastics typically suffer from reduced thermal stability, a limitation that can be mitigated through the incorporation of functional fillers like talc or metal oxides [40]. Currently, a recent study on the optimization and prediction of mechanical performance in recycled PLA filaments reported that using a 70% infill density and 0.25 mm layer thickness, followed by annealing at 75°C for 3 h, resulted in a 7.3% increase in tensile strength and a 22.3% improvement in crystallinity [41].

As mentioned, studies on the mechanical design, optimization, and enhancement of the durability of polymer-based structures produced by 3D printing through extrusion remain up-to-date. In this study, a machine learning model has been developed and trained to predict the mechanical durability of materials produced by 3D printing and to optimize design and production. While prior studies have advanced parameter-specific ML models, gaps remain in addressing anisotropic behavior, synthetic data generation, and multigeometry infill effects, challenges this study resolves through copula-augmented ML and mechanical analysis.

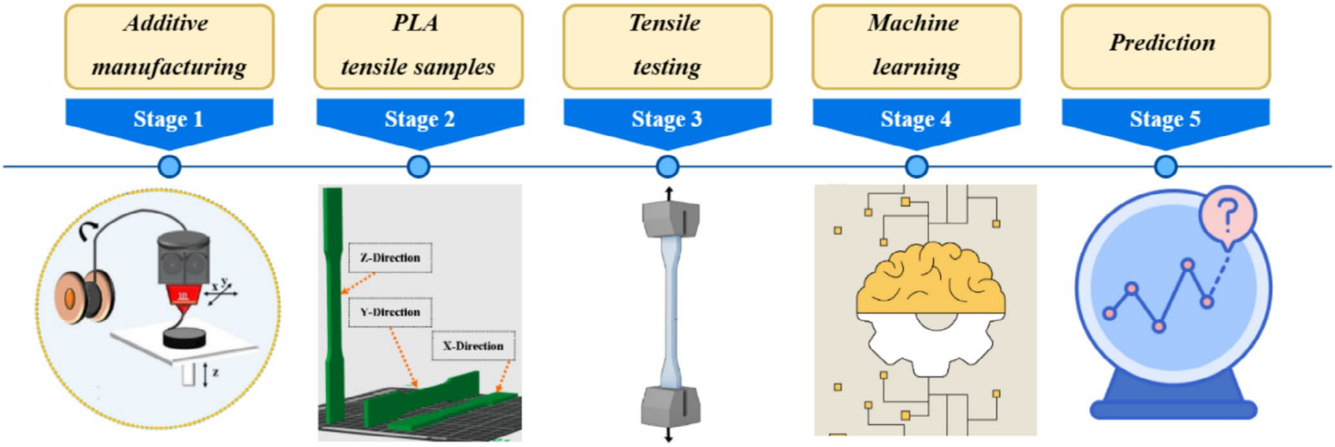

FIGURE 1 | The process of predicting the tensile strength of PLA-based samples with different filler rates using ML models. [Color figure can be viewed at wileyonlinelibrary.com]

The process steps are illustrated in Figure 1. Using the machine learning model, the tensile strengths of PLA samples with unknown infill percentages have been predicted based on four different geometries, four different infill rates, and three different print orientations.

2 | Experiments

2.1 | Preparation of Tensile Experiments

All samples in this study were produced from PLA filament according to the ASTM D638 tensile test standard. The geometries of the test samples were converted to STL format in SolidWorks 2022 before slicing in the Bambulab3D program. The geometries transferred to the 3D printer were printed using a Bambulab3D printer with the following parameters: outer wall speed of 200 mm/s, infill speed of 300 mm/s, bed temperature of 65°C, nozzle temperature of 220°C, infill percentages of 15%, 30%, 40%, and 60%, and a filament diameter of 1.75 mm. The PLA filament, supplied by the manufacturer Rizz Makine TURKEY, exhibits the following thermal and mechanical properties: The filament has a diameter of 1.75 mm and a density of 1.24 g/cm^3. Its melt flow index, measured at 210°C under a 2.16 kg load, is 6 g/10 min. In terms of mechanical performance, the PLA shows a tensile strength of 53 MPa, a flexural strength of 83 MPa, and an elongation at break of 6%. Additionally, it has a Rockwell hardness of 108 and a maximum service temperature of 55°C.

Tensile tests were conducted using a Raegen (MTS Systems) machine with a 50 kN load capacity. During the tensile testing, the samples were strained at a speed of 1 mm/min using a gripping fixture (as shown in Table 1). For each test, tensile strength, Young's modulus, elongation at break, and subsequent measurements were recorded using the MTS TestSuite TW software.

2.2 | Design of Tensile Experiments

The design parameters for the samples produced by the 3D printer include x, y, and z production directions, with gyroid, lattice, honeycomb, and linear infill geometries used in each direction, filled at 15%, 30%, 45%, and 60% infill rate (Table 2). As shown in Figure 2, a total of 48 samples were produced, using 3 printing directions, 4 infill geometries, and 4 infill rates, and were subjected to tensile testing. All the samples tested in the tensile test are shown in Figure 3. The images of the PLA-based samples before the tensile test are presented in Figure 3a, while the images after the tensile test are shown in Figure 3b.

TABLE 1 | Experiment parameter settings.

Process parameters	Units	Range
PLA content	%	100
Layer thickness	mm	—
Printing temperature	°C	220
3D printer settings	Units	Range
Printing speed	mm/s	200
Bed temperature	°C	65
Filling rate	%	15–60
Filament diameter	mm	1.75
Tensile test settings	Units	Range
Load capacity	kN	50
Stretch speed	mm/min	1

TABLE 2 | Sample parameters designed by 3D printer for tensile testing.

Fill geometry	Print direction	Filling rate (%)
Gyroid	x, y, z	15, 30, 45, 60
Lattice	x, y, z	15, 30, 45, 60
Honeycomb	x, y, z	15, 30, 45, 60
Linear	x, y, z	15, 30, 45, 60

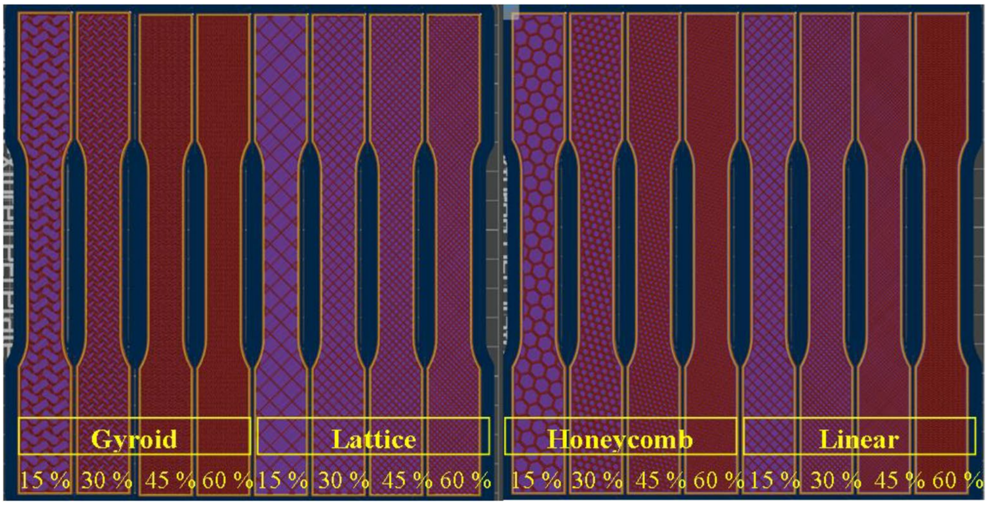

FIGURE 2 | Design of 3D-printed PLA samples with different infill rates and geometry. [Color figure can be viewed at wileyonlinelibrary.com]

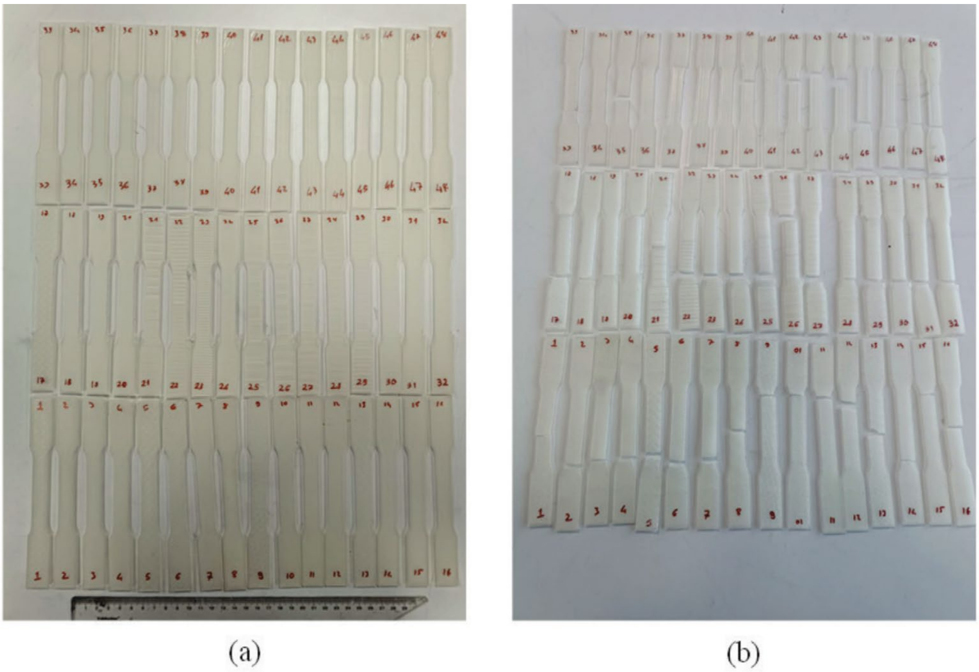

FIGURE 3 | Samples of PLA: before tensile test (a) and after tensile test (b). [Color figure can be viewed at wileyonlinelibrary.com]

2.3 | Experimental Results

Tensile tests were performed on 48 samples produced by the 3D printer, which vary according to infill geometry, infill rate, and direction, as presented in Table 2.

The mechanical values obtained from these tests were calculated and transformed into data for evaluation in machine learning models. The values for the fracture strength of the samples are shown in Table 3.

As a result of the tensile tests, the fracture strength data of all sample types were input into machine learning models for comparison, validation, replication, and prediction, using experimental values for these processes. Stress–strain graphs obtained as a result of tensile tests of PLA samples designed and produced according to infill geometry, infill rate, and printing direction were prepared, and their tensile strengths were compared. The stress–strain graphs, compared according to different printing directions and infill geometries, are presented for 15% infill in Figure 4, 30% infill in Figure 5, 45% infill in Figure 6, and 60% infill in Figure 7.

In Figure 5, the Lattice pattern has the lowest tensile strength, especially at low infill rate (43.4 MPa for 15%). In Figure 7, the honeycomb pattern provides the highest tensile strength at high infill rate (53.4 MPa for 60%). As the infill rate increases, tensile strength improves for all patterns, but the rate of increase varies depending on the pattern and print direction. Gyroid and linear patterns perform better at lower infill rates (15%–30%). The linear pattern provides the closest competition to honeycomb at

TABLE 3 | Tensile strength and strain values of PLA samples.

Sample type	Print direction	Fill rate (%)	Tensile strength (MPa)	Tensile strain (%)
Gyroid	x	15	45.1	2.03
Gyroid	x	30	47.5	1.49
Gyroid	x	45	48.7	2.03
Gyroid	x	60	50.4	1.91
Gyroid	y	15	43.6	1.16
Gyroid	y	30	44.5	1.24
Gyroid	y	45	45.9	1.40
Gyroid	y	60	47.3	1.30
Gyroid	z	15	34	0.81
Gyroid	z	30	36.4	0.79
Gyroid	z	45	39.8	1.07
Gyroid	z	60	41.8	1.06
Lattice	x	15	43.4	1.96
Lattice	x	30	46.9	1.71
Lattice	x	45	47.4	2.13
Lattice	x	60	50.2	1.65
Lattice	y	15	42	1.05
Lattice	y	30	44.1	1.40
Lattice	y	45	46.3	1.36
Lattice	y	60	47.2	1.29
Lattice	z	15	37.6	0.95
Lattice	z	30	38	0.83
Lattice	z	45	43	1.06
Lattice	z	60	44.8	1.17
Honeycomb	x	15	46.3	1.68
Honeycomb	x	30	46.2	1.35
Honeycomb	x	45	46	1.24
Honeycomb	x	60	53.4	1.71
Honeycomb	y	15	44.5	1.36
Honeycomb	y	30	45	1.31
Honeycomb	y	45	46.3	1.17
Honeycomb	y	60	49.5	1.29
Honeycomb	z	15	34.9	0.82
Honeycomb	z	30	37	0.90
Honeycomb	z	45	41	1.02
Honeycomb	z	60	40.1	0.80
Linear	x	15	44.7	1.70
Linear	x	30	47.4	1.55
Linear	x	45	49.2	1.66
Linear	x	60	49.9	1.89
Linear	y	15	43.9	1.35
Linear	y	30	44.8	1.36
Linear	y	45	45.1	1.31
Linear	y	60	50.2	1.34
Linear	z	15	37.7	0.95
Linear	z	30	39.1	1.02
Linear	z	45	40	1.07
Linear	z	60	44.3	1.18

45% and 60% infill rate (Figures 6 and 7). The Lattice pattern generally exhibits the lowest tensile strength and performs particularly poorly in the z direction.

When the tensile strength percentage changes in the infill rate change from 15% to 60% for lattice, gyroid, honeycomb, and linear infill geometries were calculated, the results varied according to the printing directions. Lattice shows a +15.67% increase in tensile strength in the x direction, with the value rising from 43.4 MPa at 15% infill rate to 50.2 MPa at 60% infill rate. Honeycomb displays a +15.33% increase in tensile strength in the x direction, with the value increasing from 46.3 MPa at 15% infill rate to 53.4 MPa at 60% infill rate. Gyroid shows a +11.75% increase in tensile strength in the x direction, with the value rising from 45.1 MPa at 15% infill rate to 50.4 MPa at 60% infill rate. Linear demonstrates a +11.63% increase in tensile strength in the x direction, with the value increasing from 44.7 MPa at 15% infill rate to 49.9 MPa at 60% infill rate.

Linear demonstrates a +14.35% strain increase in tensile strength along its y-axis as the value rises from 43.9 MPa at a 15% infill rate to 50.2 MPa at a 60% infill rate. The tensile strength in the y direction of Honeycomb structures increased by +11.24% as the infill rate rose from 15% to 60%. This change resulted in a tensile strength value rise from 44.5 to 49.5 MPa. The tensile strength in the y direction rose by +12.38% when the infill percentage increased from 42.0 MPa at 15% to 47.2 MPa at 60%. Gyroid produces the minimal tensile strength improvement of +8.49% in the y direction since the strength value increases from 43.6 MPa at a 15% infill rate to 47.3 MPa at a 60% infill rate.

Tensile strength in the z direction for gyroid structures increases by +22.94% because they transition from 34.0 MPa at

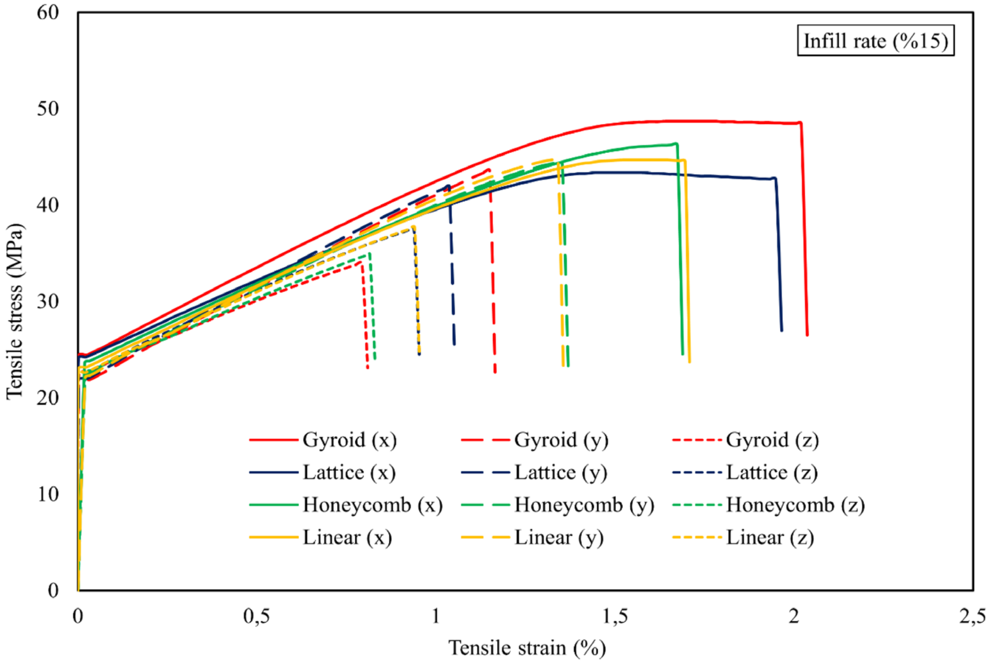

FIGURE 4 | Stress–strain curves of PLA materials with different infill geometries and printing direction at 15% infill rate. [Color figure can be viewed at wileyonlinelibrary.com]

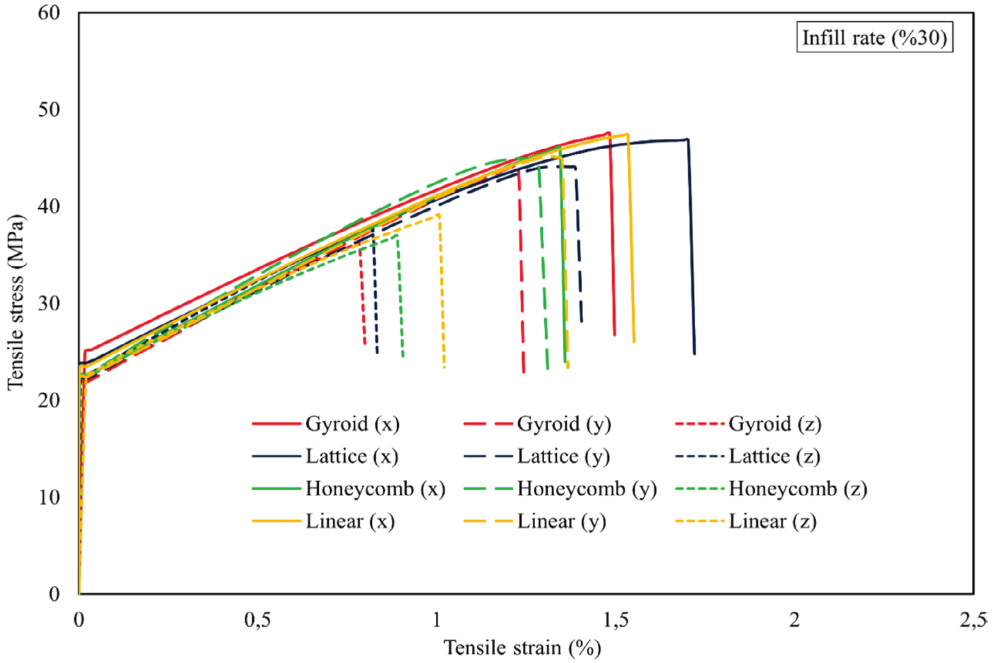

FIGURE 5 | Stress–strain curves of PLA materials with different infill geometry and printing direction at 30% infill rate. [Color figure can be viewed at wileyonlinelibrary.com]

15% infill rate to 41.8 MPa at 60% infill rate. When moving from 15% to 60% infill rate lattice shows a plus 19.15% boost in tensile strength along the *z* axis, as its strength reached from 37.6 MPa to 44.8 MPa. The tensile strength measurement of Linear structures increased by +17.51% in the *z* direction when values grew from 37.7 to 44.3 MPa during infill rate transition from 15% to 60%. The tensile strength of Honeycomb increased +14.90% when tested in the *z* direction, following the shift from 34.9 MPa at 15% infill rate to 40.1 MPa at 60% infill rate.

2.4 | Predictive Modeling With Machine Learning

2.4.1 | Copula-Based Data Augmentation

Data augmentation is a critical technique in statistical modeling and machine learning, particularly when faced with limited or imbalanced datasets. Traditional augmentation methods, such as noise injection, resampling, or geometric transformations, often focus on expanding data volume without rigorously preserving the underlying multivariate

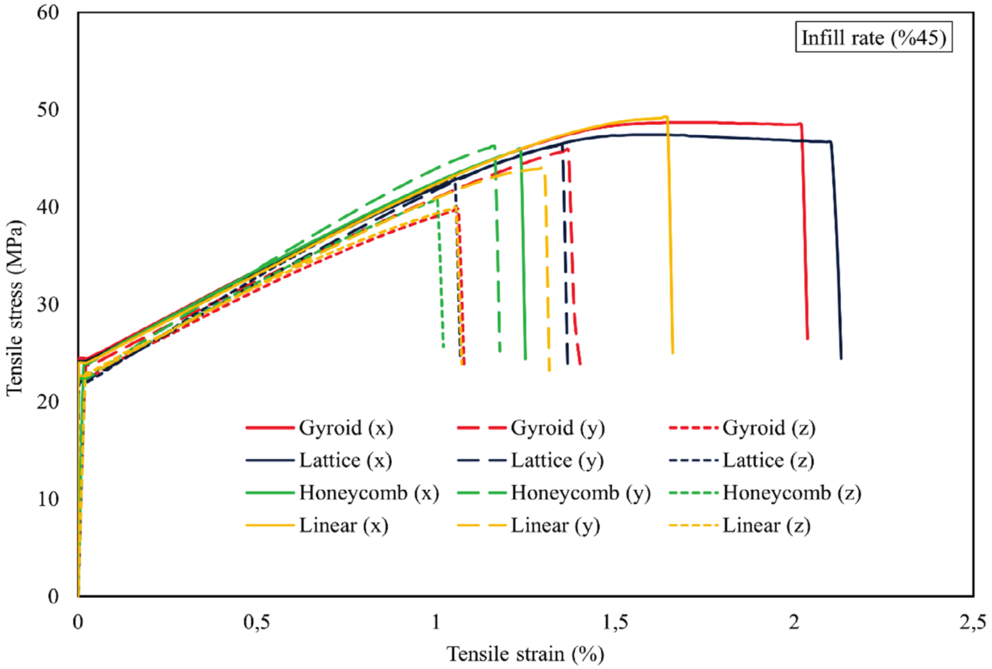

FIGURE 6 | Stress–strain curves of PLA materials with different infill geometry and printing direction at 45% infill rate. [Color figure can be viewed at wileyonlinelibrary.com]

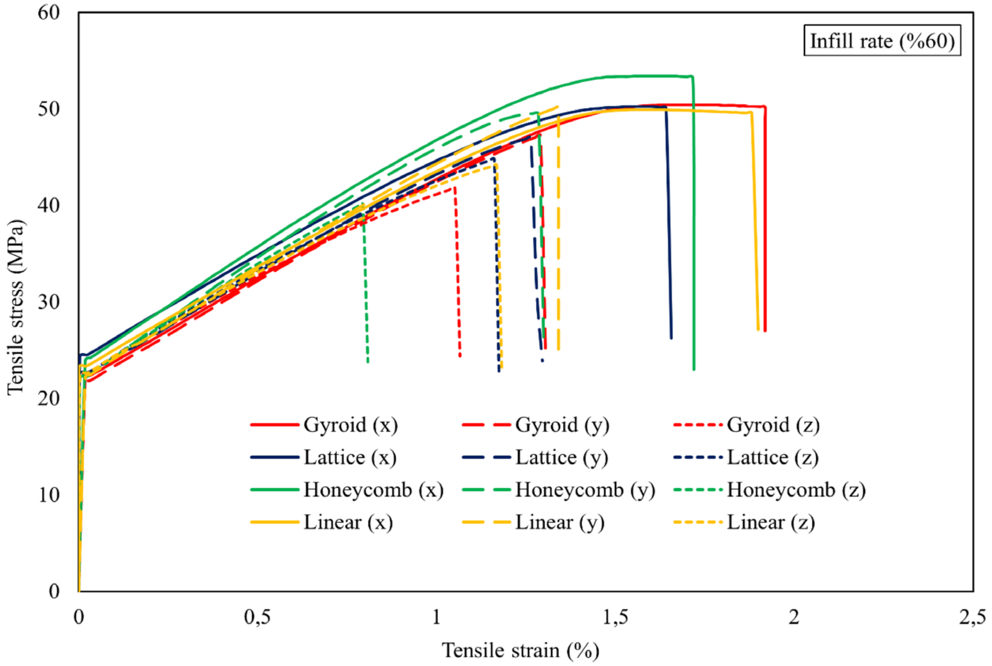

FIGURE 7 | Stress–strain curves of PLA materials with different infill geometry and printing direction at 60% infill rate. [Color figure can be viewed at wileyonlinelibrary.com]

dependencies inherent in the original dataset. The method becomes significantly limited in situations involving complex datasets, along with high dimensionality and nonlinear relationships between variables, together with tail dependencies and marginal distribution heterogeneity. Copula-based data augmentation presents itself as a reliable approach for data augmentation through its rigorous mathematical structure to generate synthetic data that maintains variable dependencies while keeping models flexible for marginal distribution fitting. The analysis investigates copula-based augmentation, which starts by examining theoretical bases and methodological approaches while discussing practical benefits compared to standard techniques [42].

The fundamental aspect of copula-based methods includes copulas as mathematical functions that describe random variable dependencies without affecting their individual distributions. The article by Sklar (1959) introduced copulas as tools that break down joint distribution functions into two distinct parts that contain individual variable marginal distributions alongside the copula function, which displays random variable relationships [43]. Formally, Sklar's theorem states that for any multivariate cumulative distribution function (*CDF*) $H(x_1, x_2, \ldots, x_d)$ with marginals $F_1, F_2, \ldots, F_d$, there exists a copula C in Equation (1).

$$H(x_1, x_2, \ldots, x_d) = C(F_1(x_1), F_2(x_2), \ldots, F_d(x_d d)) \tag{1}$$

Due to this separation of variables, modeling the dependency structure becomes possible without any limitations imposed by the choice of marginal distributions. Various popular examples of copula families include Gaussian, Clayton, Gumbel, and Student's *t*, which show different capabilities to model symmetric or asymmetric tail dependencies, thus providing diverse applications for data-generating processes.

The sequence of actions for copula-based data augmentation consists of four steps, starting with marginal distribution estimation, followed by copula selection and calibration, and then adopting synthetic uniform variables from the fitted copula before converting them to the original data scope through inverse marginal Cumulative Distribution Function transformations.

Firstly, any of parametric, nonparametric, or semiparametric methods are used to calculate the marginal distributions for each variable. Castle density estimation, together with empirical cumulative distribution functions, serves the purpose of eliminating restrictive assumptions regarding parametric models. The selection process for copula family requires observation of dependence structure. Model selection criteria, such as the Akaike information criterion (AIC), guide the choice between elliptical copulas for symmetric dependencies and Archimedean copulas for asymmetric tail dependencies. The parameters for the copula receive estimation through maximum likelihood as well as method-of-moments procedures and Bayesian techniques.

Synthetic uniform variables emerge through copula sampling of the joint distribution after its successful calibration process. These variables, which lie in the unit hypercube $[0,1]^d$, are transformed back to the original scale using the inverse CDFs of the estimated marginals. The synthesis method ensures that original univariate properties and multivariate interdependence patterns exist in synthetic data generated.

The main strength of this method is its capability to integrate different types of data values. A dataset with continuous and discrete, and ordinal variables can accept appropriate marginal distributions (gamma for continuous, Poisson for counts) while controlling variable relationships through a single copula function. The copula-based analysis provides better performance with the "curse of dimensionality" challenge than some nonparametric techniques because it represents dependence relations through few copula parameters rather than complex joint distributions.

Although copula-based augmentation brings several advantages, it still faces several difficulties in its implementation. The choice of appropriate copula family demands precise evaluation of the data dependence structure because this process becomes challenging when working with high-dimensional data. A wrong selection of copula will result in synthetic data that distorts fundamental dependencies, thus spreading analytical errors to later stages. Computationally intensive parameter estimation occurs for both large datasets and complex dependence structures found in such copulas as vine copulas. The strength of copulas exists in maintaining two-variable dependencies, but they need additional modeling to detect interactions occurring across three or more variables.

2.4.2 | Machine Learning Algorithms

The core supervised machine learning method of regression analysis seeks to develop understanding between different input variables (features) and one continuous target variable. A regression method selection depends on three critical factors, which include how the data is structured, along with the complexity of the problem, a compromise between interpretation potential and computational speed, and prediction precision. This part explores least squares regression (LSR) and support vector machines (SVMs) for regression, and Gaussian process regression (GPR), together with ANNs, as they represent leading regression approaches. The evaluation of each method includes an exploration of its theoretical foundations, together with its algorithm capabilities, as well as its advantages and constraints.

2.4.2.1 | Least Squares Regression. LSR, also known as ordinary least squares (OLS), is a foundational linear regression method that minimizes the sum of squared residuals between observed and predicted values [44]. Given a dataset with n samples and d features, the model assumes a linear relationship in Equation (2).

$$y = X\beta + \epsilon \tag{2}$$

Here, y is the target vector, X is the design matrix, β is the coefficient vector, and $\epsilon\epsilon$ represents irreducible error. The objective is to estimate β by solving the optimization problem in Equation (3).

$$\widehat{\beta} = arg \underbrace{min}_{\beta} \| y - X\beta \|_2^2 \tag{3}$$

The closed-form solution, $\widehat{\beta} = \frac{X^\top y}{(X^\top X)}$, is computationally efficient for low-to-moderate dimensional data. LSR excels in simplicity and interpretability, as coefficients directly quantify feature importance. However, its performance degrades when assumptions of linearity, homoscedasticity, and independence of errors are violated. Multicollinearity among features inflates coefficient variance, and outliers disproportionately influence squared residuals. Regularized variants like Ridge and Lasso regression address these limitations by introducing penalty terms L2 and L1 norms, respectively, to constrain coefficient magnitudes, enhancing stability and promoting sparsity.

2.4.2.2 | Support Vector Machines. SVMs, originally designed for classification, extend to regression via support vector regression (SVR). SVR seeks a function $f(x) = w^\top \phi(x) + b$ that deviates from observed targets y_i by no more than a predefined margin $\varepsilon\epsilon$, while minimizing model complexity [45]. The optimization problem is formulated as in Equations (4) and (5).

$$\underbrace{min}_{w,b} \frac{1}{2} \| w \|^2 + C \sum_{i=1}^{n} \left(\xi_i + \xi_i^*\right) \tag{4}$$

$$y_i - \left(w^\top \phi(x_i) + b\right) \le \epsilon + \xi_i, \left(w^\top \phi(x_i i) + b\right) - y_i i \le \epsilon + \xi_i^* \tag{5}$$

$$\xi i, \xi_i^* \ge 0$$

where $\xi i, \xi_i^*$ are slack variables allowing violations beyond ϵ, and C controls the trade-off between margin width and error tolerance. SVR's strength lies in its use of kernel functions to map inputs into high-dimensional spaces, enabling nonlinear regression without explicit feature engineering. It is robust to outliers due to the ϵ insensitive loss, which ignores errors smaller than $\varepsilon\epsilon$. However, performance hinges on selecting appropriate hyperparameters (C, ϵ, kernel bandwidth), and computational complexity scales cubically with dataset size, limiting scalability to large datasets.

2.4.2.3 | Gaussian Process Regression. GPR is a nonparametric, Bayesian approach that models the target function as a distribution over functions. A Gaussian process (GP) is fully specified by a mean function $m(x)$ and a covariance (kernel) function $k(x, x')$, which encodes prior assumptions about smoothness and periodicity [46]. Given training data $\{X, y\}$, the posterior predictive distribution for a test input x_* is Gaussian with mean and variance in Equations (6) and (7).

$$\mu(x_*) = k_*^\top \left(K + \sigma^2 I\right)^{-1} y \tag{6}$$

$$\sigma^2(x_*) = k(x_*, x_*) - k_*^\top \left(K + \sigma^2 I\right)^{-1} k_* \tag{7}$$

where K is the kernel matrix, k_* is the covariance vector between test and training points, and σ^2 is noise variance.

GPR provides uncertainty estimates alongside predictions, making it invaluable for applications requiring risk quantification, such as robotics and experimental design. Its flexibility stems from the kernel choice, which can be tailored to capture complex patterns. However, inference involves inverting an $n \times n$ matrix, incurring $O(n^3)$ computational cost, which becomes prohibitive for datasets exceeding several thousand samples. Sparse approximations and scalable kernels mitigate this bottleneck but introduce approximations.

2.4.2.4 | Artificial Neural Networks. ANNs are highly flexible models inspired by biological neural systems, capable of learning intricate nonlinear relationships through hierarchical feature transformations. A feedforward network comprises an input layer, multiple hidden layers, and an output layer, with each neuron applying a nonlinear activation function (e.g., ReLU, sigmoid) to its weighted inputs [47]. For regression, the output layer typically uses a linear activation, and the loss function is the mean squared error (MSE) in Equation (8).

$$L = \frac{1}{n} \sum_{i=1}^{n} \left(y_i - \hat{y}_i\right)^2 \tag{8}$$

Parameters (weights and biases) are optimized via backpropagation and gradient descent variants (e.g., Adam, RMSProp). ANNs excel in high-dimensional settings with complex interactions, such as image, speech, and text data. Deep architectures automatically extract hierarchical features, reducing reliance on manual engineering. However, they require large datasets to avoid overfitting and are computationally intensive to train. Hyperparameter tuning (e.g., layer depth, learning rate) is critical, and ANNs unlock unparalleled flexibility for large-scale problems. Techniques like dropout, batch normalization, and early stopping enhance generalization, while surrogate models provide post hoc explanations.

2.4.3 | Proposed Prediction System

The flowchart in Figure 8 illustrates a comprehensive methodology for analyzing 3D printed material tensile test data using machine learning techniques. The process is bifurcated into two primary workflows, each designed to explore different data-splitting strategies and the impact of data augmentation on model performance.

In the first workflow, the dataset, consisting of tensile test results from 3D printed materials, is divided into training and testing subsets. Seventy-five percent of the data (36 samples) is allocated for training, while the remaining 25% (12 samples) is reserved for testing. The training data is subjected to various machine learning algorithms, including LSR, SVM, GPR, and ANNs. The methods are applied separately to the training data, where they aim to deliver precise predictions of tensile properties.

The model application initiates hyperparameter optimization as the next procedural step. The integration of parameter adjustment stands as a vital step because it uses machimost recent studies on this topic was conducted bne learning algorithm parameters to optimize their prediction abilities. The grid search optimization method helped determine the best set of parameters. The optimized models receive evaluation by applying test data that was segregated from the initial project. Evaluation of models in this phase provides a report about algorithm predictive power and generalization capabilities, as well as identifies the best solution for this specific dataset.

Workflow number two embraces a differentiated method that implements both modified data split proportions and augmented data. The training data consists of 25% of the original dataset, containing 12 samples, whereas the testing data utilizes 75% comprising 36 samples. The reduced training data size limitations become minimized through a copula-based data augmentation technique. The statistical approach creates 20,000 synthetic data points, which increases both training dataset size and reduces data-related issues. The copula-based augmentation technique demonstrates outstanding capabilities to reproduce

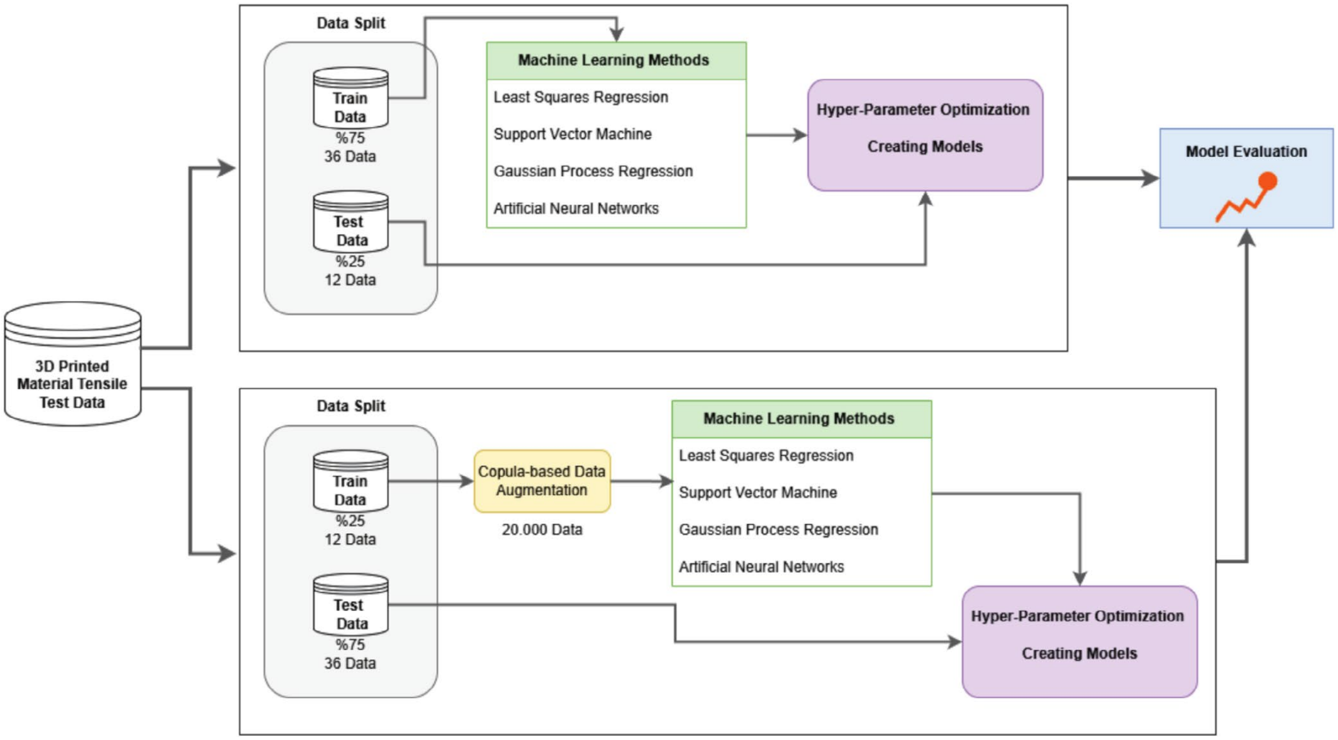

FIGURE 8 | Flowchart of the proposed tensile strength prediction system. [Color figure can be viewed at wileyonlinelibrary.com]

original data dependencies, so it creates realistic synthetic samples that represent the initial dataset accurately.

The machine learning methods LSR, SVM, GPR, and ANN analyze the data after augmentation. The workflow adopts hyperparameter optimization to adjust the models for optimal compatibility with data features of the augmented samples. When optimization completes, the models receive assessment against the larger test set to determine data augmentation effects on performance and generalization capabilities.

The methodology's last step performs a comparative evaluation of assessment results between the two workflows. The research conducts an analysis to understand data-splitting techniques and how well copula-based data augmentation supports machine learning algorithms and their predictive abilities. This research describes an orderly assessment of modeling practices, which enables the discovery of the most effective methods for tensile property modeling of 3D-printed materials, thereby advancing machine learning knowledge in materials science.

Machine learning models directed at tensile test data of 3D printed materials require hyperparameter optimization for achieving better performance. Table 4 contains detailed specifications on the chosen hyperparameters for each model type after thorough selection for accurate prediction results. Models' predictive capabilities depend on every single unique aspect shaped by the model's hyperparameters, including regularization along with kernel functions and optimization constraints, and activation functions.

The LSR kernel model requires configuration of various essential hyperparameters for operation. Least squares kernel works as the learner type because it uses a method to minimize the sum of squared residuals between predictions and actual measurements. The number of dimension expansions activates automatically in this setting to let the algorithm find optimal feature space dimensions by itself. Lambda (regularization strength) operates in automatic mode for preventing overfitting by automatically penalizing model coefficients. System adjustments of the kernel scale optimize the spread, and the built-in data standardization normalizes all features for uniform treatment of different scale ranges. The maximum number of optimization cycles is restricted to 1000 because it strikes an equilibrium between computational efficiency and model accuracy levels.

The coarse Gaussian SVM model works with Gaussian kernel functions due to their ability to find non-linear patterns in the data. The kernel scale parameter maintains a set value of 14 to determine the Gaussian function's spread while affecting how well the model connects with the provided data. The automatic setting for the box constraint finds the ideal balance by extending the class margin while reducing classification mistakes. The model can automatically adjust its error sensitivity through the automatic setup of the margin of tolerance parameter called epsilon. SVM models require standardizing data as a strategy to maintain stable features that support their operational effectiveness.

Rational quadratic GPR, as the third model, includes multiple hyperparameters that increase its flexibility, together with improved prediction precision. The baseline value for the regression function comes from the constant basis function. Rational quadratic functions as kernel show excellent performance because they adapt well to different levels of data smoothness. The model uses an isotropic kernel, which distributes a single scale factor uniformly among all dimensions to decrease the complexity level. Each automatic setting controls kernel scale, signal standard deviation, and sigma, allowing the model to calculate these parameters according to data features. The model benefits from numeric parameter optimization for hyperparameter tuning during training through standardized data processing.

TABLE 4 | Hyperparameters of the models.

Model no	Model type	Hyperparameters
1	Least squares regression kernel	Learner: Least squares kernel Number of expansion dimensions: auto Regularization strength (lambda): auto Kernel scale: auto Standardize data: yes Iteration limit: 1000
2	Coarse Gaussian SVM	Kernel function: Gaussian Kernel scale: 14 Box constraint: automatic Epsilon: auto Standardize data: yes
3	Rational quadratic GPR	Basis function: constant Kernel function: rational Quadratic Use isotropic kernel: yes Kernel scale: automatic Signal standard deviation: automatic Sigma: automatic Standardize data: yes Optimize numeric parameters: yes
4	Narrow neural network	Number of fully connected layers: 1 First layer size: 10 Activation: ReLU Iteration limit: 1000 Regularization strength (lambda): 0 Standardize data: yes

The narrow neural network serves as the fourth model, which demonstrates characteristics from its model architecture in combination with training parameters. The model architecture contains a single fully connected layer because this configuration maintains data patterns while being computationally efficient. The first layer adjoins 10 neurons while using the ReLU (rectified linear unit) activation property to achieve non-linear patterns in model learning. During training, the model will execute 1000 iterations to maintain high efficiency of its computations. The setting of Regularization strength (Lambda) to 0 indicates an absence of penalties on large weights, making it fitting for datasets that require prevention of underfitting. To maintain neural network training stability, standardization techniques must be applied to all input data sets because they help establish consistent scaling values.

The selected and optimized hyperparameters from grid search led to enhanced performance in each model to deliver precise and dependable predictions for 3D-printed material tensile properties. The performance and generality of a model depend heavily on parameter tuning because this process ensures optimal results, especially when addressing complex datasets with diverse augmentation techniques.

The performance analysis presented in Table 5 functions as the key component of this research to determine the predictive quality along with universal applicability of employed machine learning methods between original and synthetic data datasets. Multiple performance assessment metrics were used to evaluate the study thoroughly. These metrics give a detailed assessment that evaluates model accuracy, together with variance explanation as well as error distribution.

The average squared error measurement is MSE, while root mean squared error (RMSE) indicates the root-squared differences between prediction and actual values. The performance prediction improves when metric values decrease. The LSR kernel produced the most accurate predictions regarding the original data through its lowest measurement of 3.1809 MSE alongside 1.7835 RMSE. The narrow neural network produced maximum prediction mistakes by reaching an MSE value of 30.204 and a corresponding RMSE of 5.4958 when evaluating the original dataset.

TABLE 5 | Performance metrics of the proposed models on test data.

Data type	Model	MSE (test)	RMSE (test)	R^2 (test)	MAE (test)	MAPE% (test)
Original data	Least squares regression kernel	31,809	17,835	0,69,935	15,702	35,680
	Coarse Gaussian SVM	41,163	20,288	0,61,094	17,887	41,263
	Rational quadratic GPR	44,563	21,109	0,57,880	18,116	41,356
	Narrow neural network	30,204	54,958	0,18,546	47,899	10,6736
Synthetic data	Least squares regression kernel	24,321	15,595	0,87,635	12,057	28,180
	Coarse Gaussian SVM	23,463	15,317	0,88,071	12,090	28,137
	Rational quadratic GPR	24,863	15,768	0,87,359	12,104	28,277
	Narrow neural network	23,998	15,491	0,87,799	12,476	28,783

The change to synthetic data benefited all assessment models since they demonstrated better MSE and RMSE performances. The Coarse Gaussian SVM delivered the minimum possible MSE values at 2.3463, together with RMSE at 1.5317, while offering similar prediction results to the other tested models due to the addition of synthetic data. Data augmentation led to performance improvements across the Narrow Neural Network model since it processed new training data with an MSE rating of 2.3998 and an RMSE result of 1.5491.

R-squared (R^2) explains how well independent variables predict changes in dependent variables through numbers representing the proportion of variance. The LSR kernel demonstrated the maximum R^2 value of 0.69935 on the original dataset, which represented about 70% variance explained by the model. In contrast, the narrow neural network's R^2 value of 0.18546 suggested poor variance explanation and limited predictive power. When synthetic data were used, the R^2 values exceeded 0.87 and reached their highest point at 0.88071 while obtained from the coarse Gaussian SVM. The models demonstrate enhanced explanation power because of copula-based data augmentation techniques.

Mean absolute error (MAE) determines the unoriented average error size between predicted and actual values in a straightforward fashion. The LSR kernel showed the smallest MAE of 1.5702 when tested on original data because its predictions were most accurate, whereas the narrow neural network achieved the highest MAE at 4.7899, supporting other evaluation results. All models in the synthetic dataset achieved decreased MAE values, where the LSR kernel exhibited the best performance with 1.2057 as the minimum value. Model predictions show enhanced reliability when the error magnitude diminishes regularly across all models due to augmented data implementation.

The normalized predictive accuracy assessment through Mean Absolute Percentage Error (MAPE) provides metric results as percentage values, which enable comparison of various models' accuracy. The original data analysis revealed LSR kernel as the top performer with 3.5680% MAPE, but the narrow neural network delivered inconsistent results with a higher 10.6736% MAPE. The MAPE measurements demonstrated substantial reduction when synthetic data was introduced to the models, where the Coarse Gaussian SVM produced the best value at 2.8137%. The effectiveness of data augmentation becomes apparent through this data, which demonstrates more dependable and consistent prediction capabilities.

The LSR kernel achieved better performance across the original dataset, yet the Coarse Gaussian SVM showed a minor advantage over other models on synthetic data. Using copula-based data augmentation improved model performance for every model and created substantial enhancements in the Narrow Neural Network that demonstrated inferior results before augmentation. The study shows how data augmentation is essential in machine learning operations when handling small datasets, while demonstrating that selecting proper model settings leads to the best prediction results.

The experimental results, illustrated in Figures 9 and 10, performance of four regression models is compared. Models trained on copula-augmented data demonstrate stable performance on the larger test set, suggesting reduced overfitting. The figures highlight the transformative potential of copula-based data augmentation in regression tasks. By expanding a small training set into a diverse synthetic dataset (20,000 samples), all models achieve enhanced generalization and stability. These results advocate for copula methods in scenarios with limited labeled data, provided the synthetic data accurately reflects the underlying data-generating process.

2.5 | Prediction of Tensile Strength

Figures 11, 12, and 13 present the predicted tensile strength for various infill patterns (gyroid, lattice, honeycomb, and linear) across the *x*, *y*, and *z* directions of 3D-printed PLA specimens. These predictions were obtained using an SVM model that was trained on experimentally measured data at 15%, 30%, 45%, and 60% infill rates, supplemented with copula-based data augmentation. By leveraging only 25% of the real tensile test results, the model was trained and then tested on the remaining 75% of the data, showing strong predictive performance. Subsequently, the same model was used to extrapolate tensile strengths at intermediate and higher fill rates (from 15% to 90%), yielding nearly linear trends for all infill patterns. Although the tensile strength generally increases with fill rate in each direction, there are subtle differences among the four infill geometries, with gyroid and lattice patterns often yielding slightly higher strength than honeycomb and linear patterns. The directional behavior highlights the inherent anisotropy of FFF, as the *x* and *y* directions tend to exhibit marginally higher strengths than the *z* direction. Overall, these results underscore the SVM model's ability to capture both the effect of fill rate and the influence of infill geometry on tensile performance, offering a comprehensive view of how these parameters can be optimized for improved mechanical properties. The predicted tensile test results (for 15% to 90% fill rate) reveal critical insights into the relationships between printing direction, infill pattern, fill rate, and tensile strength. Across all configurations, fill rate exhibits a consistent positive correlation with tensile strength. For example, at 15% fill rate, the gyroid pattern in the *x*-direction yields a tensile strength of 47.54 MPa, while increasing the fill rate to 90% enhances this value to 54.58 MPa. This trend holds for all patterns and printing directions, underscoring the importance of higher material density in improving mechanical performance.

Printing direction significantly influences tensile strength, with the *x*-direction consistently outperforming *y*- and *z*-directions. For instance, at a 30% fill rate, the gyroid pattern achieves 48.83 MPa (*x*-direction) versus 45.23 MPa (*y*-direction) and 41.08 MPa (*z*-direction). This anisotropy likely stems from layer adhesion dynamics and filament alignment during printing, where stresses parallel to the deposition plane are better accommodated than those perpendicular (*z*). The *z*-direction's lower strength highlights a critical limitation in applications requiring isotropic properties.

Among infill patterns, gyroid demonstrates superior tensile strength compared to lattice, honeycomb, and linear. For example, at a 50.625% fill rate, gyroid (*x*-direction) achieves

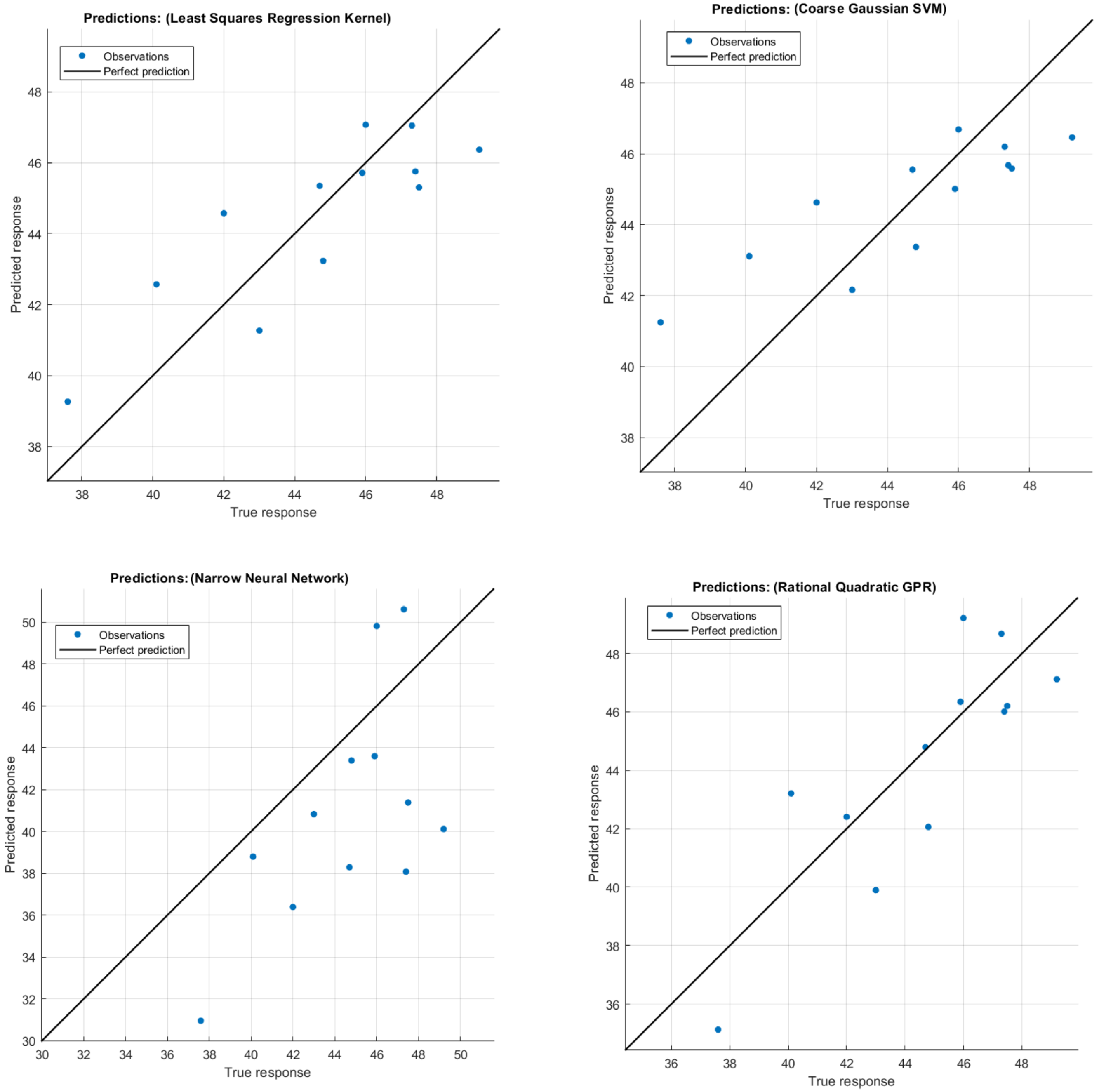

FIGURE 9 | Predictions and test data on original data training, least squares regression, support vector regression, Gaussian process regression, and artificial neural networks, respectively. [Color figure can be viewed at wileyonlinelibrary.com]

50.55 MPa, while Linear (*x*-direction) reaches 49.34 MPa. The gyroid's interconnected lattice structure may distribute stress more uniformly, whereas linear patterns (linear) exhibit directional weaknesses. However, the marginal differences between gyroid and lattice (e.g., 47.71 vs. 47.64 MPa at 16.875% fill rate in the *x*-direction) suggest that pattern selection can be tailored to balance strength with printing efficiency or material usage.

The data supports the use of high fill rates for applications demanding maximum strength, albeit at the cost of increased material consumption. The gyroid pattern's performance positions it as advantageous for load-bearing components, while the *x*-direction's robustness validates its use in primary stress-aligned designs. Additionally, the linear scalability of strength with fill rate simplifies predictive modeling for structural optimization. The pronounced anisotropy between printing directions limits the reliability of *z*-oriented components, necessitating design compensations such as reinforcement or multiaxis printing. While gyroid excels, its complex geometry may increase printing time and computational overhead compared to simpler patterns like Linear. Furthermore, the diminishing returns in strength gain at higher fill rates (e.g., 75%–90% fill rate for gyroid in *x*-direction improves strength by only ~7%) question the cost-effectiveness of maximal infill in noncritical applications.

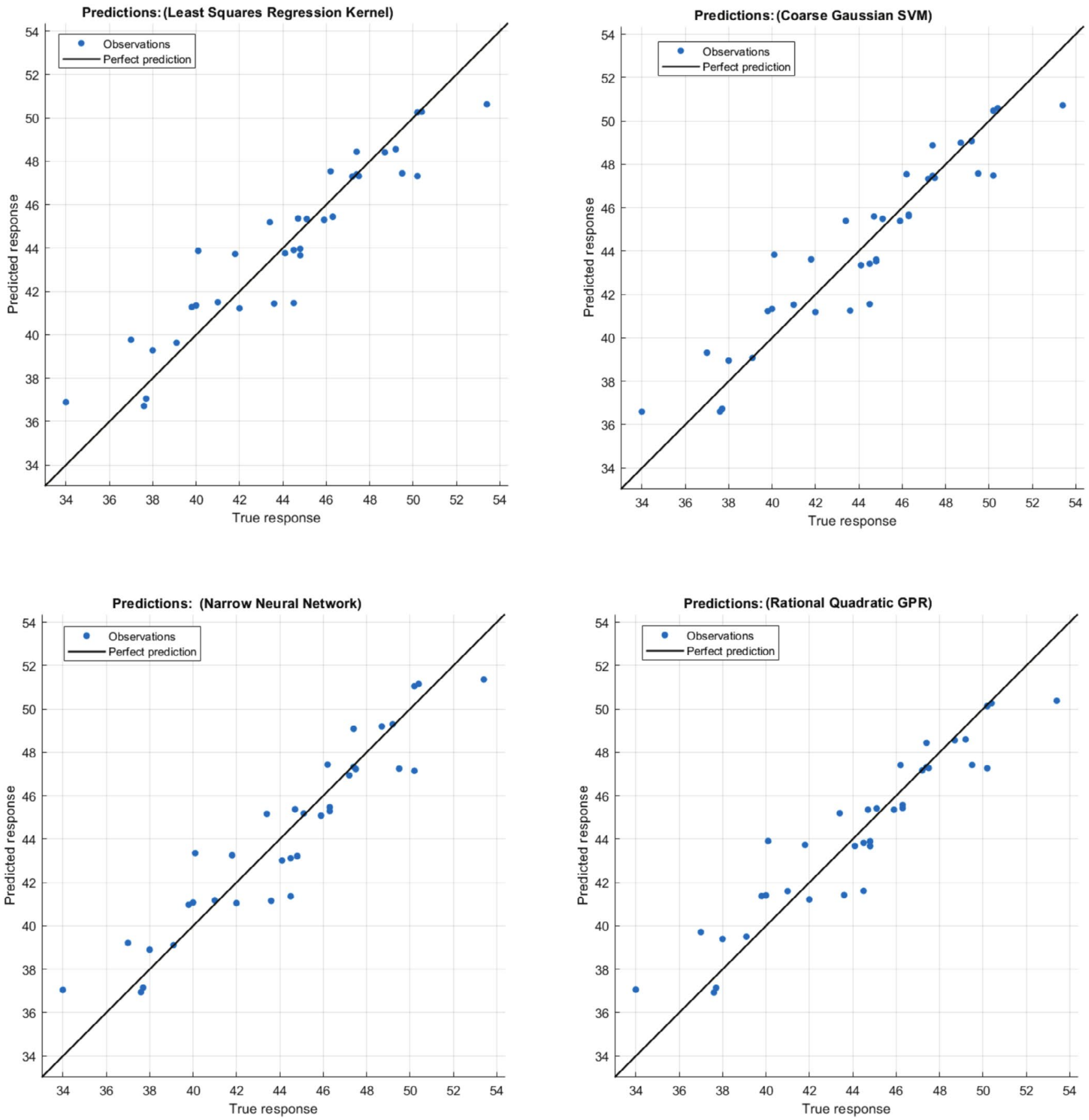

FIGURE 10 | Predictions and test data on synthetic data training, least squares regression, support vector regression, Gaussian process regression, and artificial neural networks, respectively. [Color figure can be viewed at wileyonlinelibrary.com]

3 | Conclusion and Prospects

The analysis of tensile strength variations across different infill patterns and print directions reveals that the highest percentage increase in tensile strength is observed in the gyroid structure along the *z* direction, with a 22.94% increase from 15% to 60% infill rate. This indicates that, despite generally lower tensile strength in the *z* direction, the increase in infill rate significantly enhances mechanical performance in this orientation. In contrast, the lowest percentage increase is recorded for the gyroid structure in the *Y* direction, with only an 8.49% improvement, suggesting that increasing infill density has a comparatively lower impact on strengthening the material along this axis. Additionally, the *z* direction consistently demonstrates the largest percentage variations in tensile strength across all infill patterns, implying a higher sensitivity to infill rate changes due to the inherent layer-by-layer deposition nature of AM. The mechanical response of the 3D-printed components remains stable as the *x* and *y* directions show lesser percentage increases compared to the z direction. Print orientation, together with infill

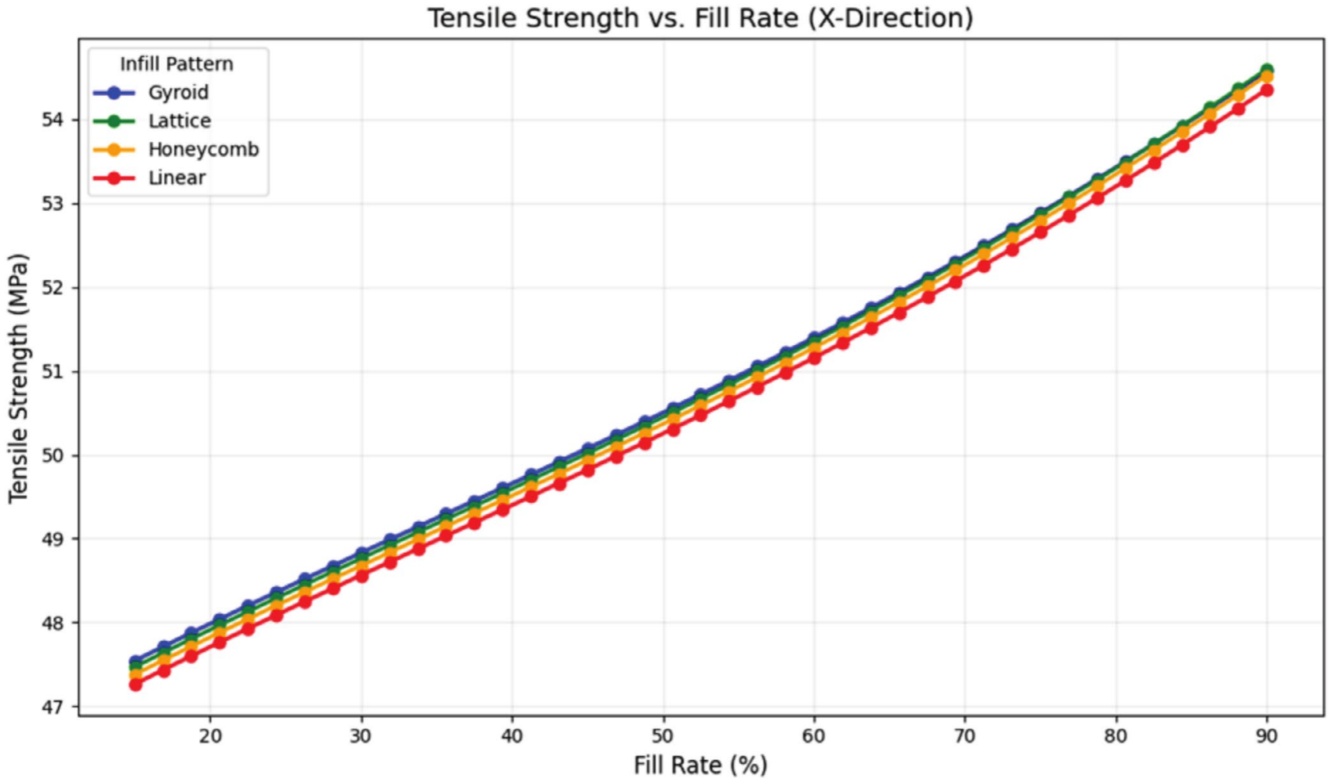

FIGURE 11 | Tensile strength predictions with SVM model in *x*-direction. [Color figure can be viewed at wileyonlinelibrary.com]

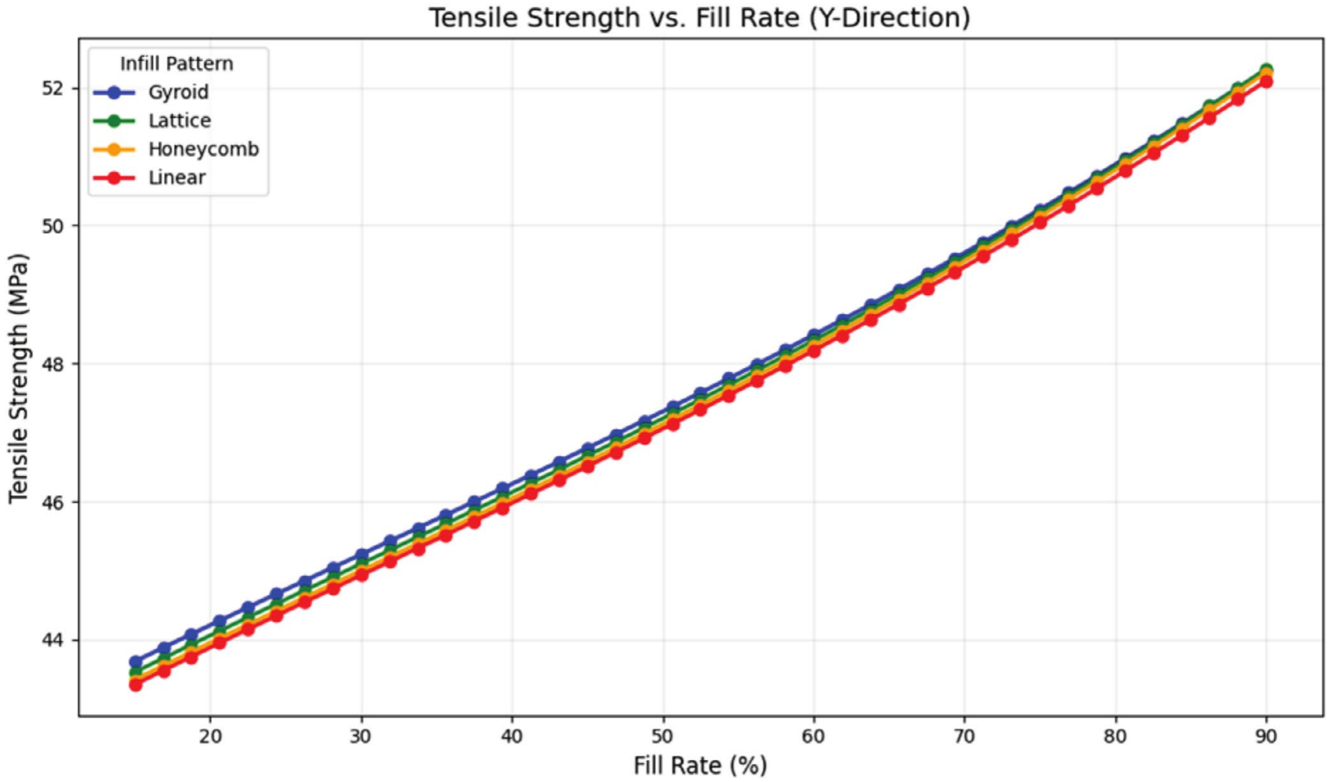

FIGURE 12 | Tensile strength predictions with SVM model in *y*-direction. [Color figure can be viewed at wileyonlinelibrary.com]

pattern, significantly affects the mechanical properties of 3D-printed PLA components, so designers must carefully select parameters for optimal performance.

Results from the Machine Learning predictions showed that mechanical anisotropy reaches maximum performance by printing gyroid patterns in the *x*-direction. The *z*-direction experienced

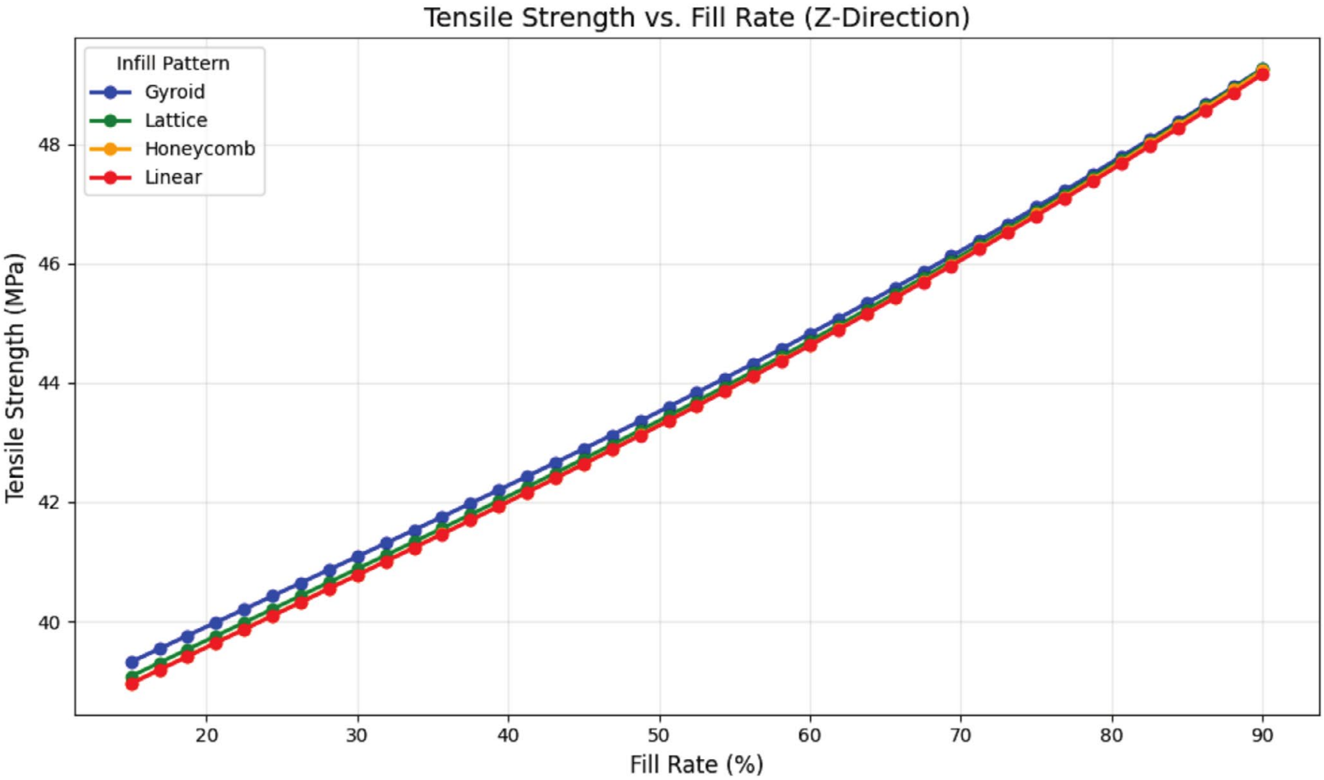

FIGURE 13 | Tensile strength predictions with SVM model in z-direction. [Color figure can be viewed at wileyonlinelibrary.com]

the greatest improvement in tensile strength among all directions due to its high sensitivity toward infill density despite the material's weak layer adhesion properties. The machine learning models trained using copula-augmented data achieved high accuracy levels, so SVM and ANN predictions maintained MAPE values less than 3% thus demonstrating their value in parameter optimization problems.

For structural load-bearing purposes, one should use high infill rates within gyroid geometries alongside x-direction printing to achieve maximum strength levels. The performance requirements should be considered during material usage decisions when infill rates exceed 75%. Researchers should investigate printing across multiple axes in future work to improve z-direction performance because predictive models need incorporation of environmental elements. This framework holds potential to expand its industrial usefulness when researchers apply it to study fatigue behavior and impact resistance. This research establishes a link between experimental data and machine learning, which enables intelligent manufacturing by leading to fast prototyping while promoting sustainable material usage.

One of the most recent studies on this topic was conducted by Asad et al. [48], who developed a hybrid deep learning—Taguchi optimization framework—and successfully predicted the tensile strength of PLA with 95.2% accuracy using a limited number of geometric parameters and process settings. Similarly, Qayyum et al. [49] employed the Random Forest algorithm to predict the flexural behavior of carbon fiber-reinforced PLA composites using only 550 data points, achieving $R^2=0.99$ and RMSE = 1.17. While both studies present valuable contributions, they either rely on isotropic material assumptions or limit their analyses to specific fiber-reinforced systems, thus overlooking the challenges of directional anisotropy and data scarcity. In contrast, the present study utilized 48 experimental specimens produced with four distinct infill geometries and three orthogonal printing directions, capturing anisotropic mechanical behavior and enhancing model learning through 20,000 copula-based synthetic data points that preserve multivariate dependency structures. As a result, GPR and SVM models trained with only 25% real data achieved high predictive performance, with RMSE as low as 1.53 MPa and R^2 exceeding 0.87. These findings demonstrate that the proposed model is not only generalizable under anisotropic conditions but also capable of delivering high-accuracy predictions in standard PLA systems without fiber reinforcement, even when limited and heterogeneous datasets are available.

In future applications, this approach can be extended to predict the behavior of direction-dependent structural components under multiaxial loading, estimate performance variability in parts made from recycled materials, or model time-dependent changes in mechanical properties under environmental influences. Accordingly, it offers a data-driven foundation to enhance the numerical accuracy of low-cost and environmentally sustainable prototyping processes.

Author Contributions

Ahmet Saylık: conceptualization (lead), data curation (equal), methodology (equal), project administration (equal), resources (lead), validation (equal), visualization (lead), writing – original draft (lead), writing – review and editing (lead). **Ertan Kösedağ:** conceptualization (lead), data curation (supporting), funding acquisition (equal), methodology (equal), validation (equal), writing – original draft (supporting),

writing – review and editing (equal). **Taha Etem:** conceptualization (lead), data curation (lead), methodology (equal), resources (supporting), validation (lead), visualization (equal), writing – original draft (equal), writing – review and editing (equal).

Acknowledgments

The authors have nothing to report.

Ethics Statement

The authors have nothing to report.

Consent

The authors have nothing to report.

Conflicts of Interest

The authors declare no conflicts of interest.

Data Availability Statement

The authors have nothing to report.

References

1. B. Mallikarjuna, P. Bhargav, S. Hiremath, K. G. Jayachristiyan, and N. Jayanth, "A Review on the Melt Extrusion-Based Fused Deposition Modeling (FDM): Background, Materials, Process Parameters and Military Applications," *International Journal of Interactive Design and Manufacturing* 19 (2023): 651–665, https://doi.org/10.1007/S12008-023-01354-0.

2. A. A. Elsonbaty, A. Mrashad, O. Y. Abass, T. Y. Abdelghany, and A. Malfauiomy, "A Survey of Fused Deposition Modeling (FDM) Technology in 3D Printing," 26, no. 11 (2024): 304–312.

3. M. Ahmad, M. Javaid, and A. Haleem, "A Study on Fused Deposition Modeling (FDM) and Laser-Based Additive Manufacturing (LBAM) in the Medical Field," *Intelligent Pharmacy* 2, no. 3 (2024): 381–391, https://doi.org/10.1016/J.IPHA.2024.02.010.

4. C. Valean, D. I. Stoia, C. Opris, and E. Linul, "Effect of Fillers on Mechanical Properties of FDM Printed PLA Components," *Procedia Structural Integrity* 56, no. 3 (2024): 97–104, https://doi.org/10.1016/j.prostr.2024.02.043.

5. N. Shahrubudin, T. C. Lee, and R. Ramlan, "An Overview on 3D Printing Technology: Technological, Materials, and Applications," *Procedia Manufacturing* 35 (2019): 1286–1296, https://doi.org/10.1016/j.promfg.2019.06.089.

6. T. R. Arunprasand and P. Nallasamy, "Advancements in Optimizing Mechanical Performance of 3d Printed Polymer Matrix Composites via Microstructural Refinement and Processing Enhancements: A Comprehensive Review," *Mechanics of Advanced Materials and Structures* (2024): 1–19, https://doi.org/10.1080/15376494.2024.2426776.

7. H. Ye, P. Mao, W. He, J. Li, Y. Dong, and X. Wang, "Influence of Process Parameters on the Tensile Properties of CFRTP Composites 3D Printed Structures," *Mechanics of Advanced Materials and Structures* (2024): 1–13, https://doi.org/10.1080/15376494.2024.2440632.

8. A. Nazir, O. Gokcekaya, K. Md Masum Billah, et al., "Multi-Material Additive Manufacturing: A Systematic Review of Design, Properties, Applications, Challenges, and 3D Printing of Materials and Cellular Metamaterials," *Materials and Design* 226 (2023): 111661, https://doi.org/10.1016/J.MATDES.2023.111661.

9. N. K. Bankapalli, V. Gupta, P. Saxena, A. Bajpai, C. Lahoda, and J. Polte, "Filament Fabrication and Subsequent Additive Manufacturing, Debinding, and Sintering for Extrusion-Based Metal Additive Manufacturing and Their Applications: A Review," *Composites. Part B, Engineering* 264 (2023): 110915, https://doi.org/10.1016/j.compositesb.2023.110915.

10. O. Bouzaglou, O. Golan, and N. Lachman, "Process Design and Parameters Interaction in Material Extrusion 3D Printing: A Review," *Polymers* 15, no. 10 (2023): 2280, https://doi.org/10.3390/polym15102280.

11. M. Sadaf, M. Bragaglia, L. Slemenik Perše, and F. Nanni, "Advancements in Metal Additive Manufacturing: A Comprehensive Review of Material Extrusion With Highly Filled Polymers," *Journal of Manufacturing and Materials Processing* 8, no. 1 (2024): 14, https://doi.org/10.3390/jmmp8010014.

12. X. Sun, M. Mazur, and C. T. Cheng, "A Review of Void Reduction Strategies in Material Extrusion-Based Additive Manufacturing," *Additive Manufacturing* 67 (2023): 103463, https://doi.org/10.1016/J.ADDMA.2023.103463.

13. Y. Zhang, L. Zhang, W. Xu, et al., "Design, Mechanical Behavior, and 3D Printing Defects of a Variable Density Lattice Compressor Impeller," *Mechanics of Advanced Materials and Structures* (2025): 1–17, https://doi.org/10.1080/15376494.2025.2455509.

14. N. Feng, Y. Tie, S. Wang, J. Guo, and Z. Hu, "Mechanical Performance of 3D-Printing Annular Honeycomb With Tailorable Poisson's Ratio," *Mechanics of Advanced Materials and Structures* 30, no. 18 (2023): 3781–3789, https://doi.org/10.1080/15376494.2022.2083733.

15. F. Ghorbani, H. Gharehbaghi, A. Farrokhabadi, A. Bolouri, A. H. Behravesh, and S. K. Hedayati, "Investigation of Energy Absorption Performances of a 3D Printed Fiber-Reinforced Bio-Inspired Cellular Structure Under In-Plane Compression Loading," *Mechanics of Advanced Materials and Structures* 31, no. 21 (2024): 5234–5252, https://doi.org/10.1080/15376494.2023.2214552.

16. I. Malashin, I. Masich, V. Tynchenko, et al., "Machine Learning in 3D and 4D Printing of Polymer Composites: A Review," *Polymers* 16, no. 22 (2024): 1–52, https://doi.org/10.3390/polym16223125.

17. M. Jayasudha, M. Elangovan, M. Mahdal, and J. Priyadarshini, "Accurate Estimation of Tensile Strength of 3D Printed Parts Using Machine Learning Algorithms," *PRO* 10 (2022): 1158, https://doi.org/10.3390/pr10061158.

18. A. Mishra, V. S. Jatti, E. Messele Sefene, et al., "Machine Learning-Assisted Pattern Recognition Algorithms for Estimating Ultimate Tensile Strength in Fused Deposition Modelled Polylactic Acid Specimens," *Materials and Technologies* 39, no. 1 (2024): 2295089, https://doi.org/10.1080/10667857.2023.2295089.

19. A. Ziadia, M. Habibi, and S. Kelouwani, "Machine Learning Study of the Effect of Process Parameters on Tensile Strength of FFF PLA and PLA-CF," *Eng* 4, no. 4 (2023): 2741–2763, https://doi.org/10.3390/ENG4040156.

20. H. Wei, L. Tang, H. Qin, et al., "Optimizing FDM 3D Printing Parameters for Improved Tensile Strength Using the Takagi–Sugeno Fuzzy Neural Network," *Materials Today Communications* 38 (2024): 108268, https://doi.org/10.1016/J.MTCOMM.2024.108268.

21. R. V. Pazhamannil, P. Govindan, and P. Sooraj, "Prediction of the Tensile Strength of Polylactic Acid Fused Deposition Models Using Artificial Neural Network Technique," *Materials Today Proceedings* 46 (2021): 9187–9193, https://doi.org/10.1016/J.MATPR.2020.01.199.

22. A. D. Tura, H. G. Lemu, H. B. Mamo, and A. J. Santhosh, "Prediction of Tensile Strength in Fused Deposition Modeling Process Using Artificial Neural Network and Fuzzy Logic," *Progress in Additive Manufacturing* 8, no. 3 (2023): 529–539, https://doi.org/10.1007/S40964-022-00346-Y/FIGURES/8.

23. S. Gao, Y. Wang, Y. Zhou, and H. Yu, "An Improved Scheduling Approach for Multi-Energy Microgrids Considering Scenario Insufficiency and Computational Complexity," *PRO* 13, no. 2 (2025): 576, https://doi.org/10.3390/PR13020576.

24. Z. Zeng, Y. Zhou, S. Wen, and C. Zhou, "Predicting the Tensile Properties of Wood Plastic Composites Using Material Extrusion With Meta-Based Few-Shot Learning," *Composites. Part A, Applied Science and Manufacturing* 190 (2025): 108671, https://doi.org/10.1016/J.COMPOSITESA.2024.108671.

25. A. Karimi, D. Rahmatabadi, and M. Baghani, "Various FDM Mechanisms Used in the Fabrication of Continuous-Fiber Reinforced Composites: A Review," *Polymers* 16, no. 6 (2024): 831, https://doi.org/10.3390/polym16060831.

26. Z. Wawryniuk, E. Brancewicz-Steinmetz, and J. Sawicki, "Revolutionizing Transportation: An Overview of 3D Printing in Aviation, Automotive, and Space Industries," *International Journal of Advanced Manufacturing Technology* 134, no. 7–8 (2024): 3083–3105, https://doi.org/10.1007/s00170-024-14226-y.

27. B. Ozdemir, M. Hernández-del-Valle, M. Gaunt, et al., "Toward 3D Printability Prediction for Thermoplastic Polymer Nanocomposites: Insights From Extrusion Printing of PLA-Based Systems," *Additive Manufacturing* 95 (2024): 104533, https://doi.org/10.1016/J.ADDMA.2024.104533.

28. A. Hamrani, A. Agarwal, A. Allouhi, and D. McDaniel, "Applying Machine Learning to Wire Arc Additive Manufacturing: A Systematic Data-Driven Literature Review," *Journal of Intelligent Manufacturing* 35, no. 6 (2023): 2407–2439 2023, https://doi.org/10.1007/S10845-023-02171-8.

29. Z. Zhang, C. K. Sahu, S. K. Singh, R. Rai, Z. Yang, and Y. Lu, "Machine Learning Based Prediction of Melt Pool Morphology in a Laser-Based Powder Bed Fusion Additive Manufacturing Process," *International Journal of Production Research* 62 (2024): 1803–1817, https://doi.org/10.1080/00207543.2023.2201860.

30. A. I. Saimon, E. Yangue, X. Yue, Z. J. Kong, and C. Liu, "Advancing Additive Manufacturing Through Deep Learning: A Comprehensive Review of Current Progress and Future Challenges," *IISE Transactions* (2024): 2443592, https://doi.org/10.1080/24725854.2024.2443592.

31. M. Karimzadeh, D. Basvoju, A. Vakanski, I. Charit, F. Xu, and X. Zhang, "Review of Machine Learning Methods for Additive Manufacturing of Functionally Graded Materials," *Materials* 17, no. 15 (2023): ma17153673, https://doi.org/10.3390/ma17153673.

32. A. Peles, V. C. Paquit, and R. R. Dehoff, "Deep-Learning Quantitative Structural Characterization in Additive Manufacturing," 2023, https://arxiv.org/abs/2302.06389v1.

33. K. H. Kazmi, M. Chandra, S. Rajak, S. K. Sharma, A. Mandal, and A. K. Das, "Implementing Machine Learning in Robotic Wire Arc Additive Manufacturing for Minimizing Surface Roughness," *International Journal of Computer Integrated Manufacturing* 38 (2025): 255–270, https://doi.org/10.1080/0951192X.2024.2330091.

34. S. Kumar, T. Gopi, N. Harikeerthana, et al., "Machine Learning Techniques in Additive Manufacturing: A State of the Art Review on Design, Processes and Production Control," *Journal of Intelligent Manufacturing* 34, no. 1 (2022): 21–55, https://doi.org/10.1007/S10845-022-02029-5.

35. S. L. Sing, C. N. Kuo, C. T. Shih, C. C. Ho, and C. K. Chua, "Perspectives of Using Machine Learning in Laser Powder Bed Fusion for Metal Additive Manufacturing," *Virtual and Physical Prototyping* 16, no. 3 (2021): 372–386, https://doi.org/10.1080/17452759.2021.1944229.

36. J. Jiang, "A Survey of Machine Learning in Additive Manufacturing Technologies," *International Journal of Computer Integrated Manufacturing* 36, no. 9 (2023): 1258–1280, https://doi.org/10.1080/0951192X.2023.2177740.

37. S. Zhao, Y. Shi, C. Huang, et al., "Integrating Machine Learning Into Additive Manufacturing of Metallic Biomaterials: A Comprehensive Review," *Journal of Functional Biomaterials* 16, no. 3 (2025): 77, https://doi.org/10.3390/JFB16030077.

38. G. Atakok, M. Kam, and H. B. Koc, "Tensile, Three-Point Bending and Impact Strength of 3D Printed Parts Using PLA and Recycled PLA Filaments: A Statistical Investigation," *Journal of Materials Research and Technology* 18 (2022): 1542–1554, https://doi.org/10.1016/J.JMRT.2022.03.013.

39. Ü. Çevik and M. Kam, "A Review Study on Mechanical Properties of Obtained Products by FDM Method and Metal/Polymer Composite Filament Production," *Journal of Nanomaterials* 2020, no. 1 (2020): 6187149, https://doi.org/10.1155/2020/6187149.

40. G. Atakok, M. Kam, and H. B. Koc, "A Review of Mechanical and Thermal Properties of Products Printed With Recycled Filaments for Use in 3D Printers," *Surface Review and Letters* 29, no. 2 (2021): 2230002, https://doi.org/10.1142/S0218625X22300027.

41. M. Tănase, A. I. Portoacă, A. Diniță, et al., "Optimizing Mechanical Properties of Recycled 3D-Printed PLA Parts for Sustainable Packaging Solutions Using Experimental Analysis and Machine Learning," *Polymer* 16, no. 23 (2024): 3268, https://doi.org/10.3390/POLYM16233268.

42. M. Nai Ruscone, D. Fernández, and A. D'Ambrosio, "Copula-Based Non-Metric Unfolding on Augmented Data Matrix," *Journal of Classification* 41, no. 3 (2024): 678–697, https://doi.org/10.1007/S00357-024-09495-X/FIGURES/5.

43. G. Geenens, "(Re-)Reading Sklar (1959)—A Personal View on Sklar's Theorem," *Mathematika* 12, no. 3 (2024): 380, https://doi.org/10.3390/MATH12030380.

44. H. Long, T. Chen, H. Chen, X. Zhou, and W. Deng, "Principal Space Approximation Ensemble Discriminative Marginalized Least-Squares Regression for Hyperspectral Image Classification," *Engineering Applications of Artificial Intelligence* 133 (2024): 108031, https://doi.org/10.1016/J.ENGAPPAI.2024.108031.

45. A. Yeganeh, S. A. Abbasi, S. C. Shongwe, J. C. Malela-Majika, and A. R. Shadman, "Evolutionary Support Vector Regression for Monitoring Poisson Profiles," *Soft Computing* 28, no. 6 (2024): 4873–4897, https://doi.org/10.1007/s00500-023-09047-2.

46. B. Jin and X. Xu, "Forecasting Wholesale Prices of Yellow Corn Through the Gaussian Process Regression," *Neural Computing & Applications* 36, no. 15 (2024): 8693–8710, https://doi.org/10.1007/S00521-024-09531-2.

47. W. Jiang, H. Han, M. He, and W. Gu, "ML-Based Pre-Deployment SDN Performance Prediction With Neural Network Boosting Regression," *Expert Systems With Applications* 241 (2024): 122774, https://doi.org/10.1016/J.ESWA.2023.122774.

48. M. H. Nikzad, M. Heidari-Rarani, R. Rasti, and P. Sareh, "Machine Learning-Driven Prediction of Tensile Strength in 3D-Printed PLA Parts," *Expert Systems With Applications* 264 (2025): 125836, https://doi.org/10.1016/J.ESWA.2024.125836.

49. H. Qayyum, K. Saqib, G. Hussain, and M. Alkahtani, "Predicting Flexural Properties of 3D-Printed Composites: A Small Dataset Analysis Using Multiple Machine Learning Models," *Materials Today Communications* 42 (2025): 111135, https://doi.org/10.1016/J.MTCOMM.2024.111135.